Diagnostic performance of contrast-enhanced computed tomography in the immediate assessment of radiofrequency ablation success in colorectal liver metastases

Christina Schraml,[1] Stephan Clasen,[1] Nina F. Schwenzer,[1] Ingmar Koenigsrainer,[2] Tina Herberts,[3] Claus D. Claussen,[1] Philippe L. Pereira[1]

[1]Department of Diagnostic and Interventional Radiology, University Hospital of Tuebingen, Hoppe-Seyler-Str. 3, Tuebingen, 72076, Germany
[2]Department of Abdominal Surgery, University Hospital of Tuebingen, Hoppe-Seyler-Str. 3, Tuebingen, 72076, Germany
[3]Department of Medical Biometry, University Hospital of Tuebingen, Westbahnhofstrasse 55, Tuebingen, 72070, Germany

Abstract

Background: To determine the accuracy of contrast-enhanced multislice computed tomography (CT) in the assessment of treatment success immediately after CT-guided radiofrequency (RF) ablation.
Methods: 26 patients with 38 Colorectal liver metastasis (CRM) were treated by CT-guided RF ablation. Precontrast and portal phase CT features before and immediately after ablation were retrospectively evaluated quantitatively and qualitatively: Influence of attenuation characteristics, safety margin, congruency between tumor and coagulation, and morphological criteria (shape, margin distinction, margin configuration, and margin continuity) were investigated. Findings were statistically analyzed with regard to local tumor progression.
Results: Mean observation period for follow-up scans was 6.4 months (range: 3–40 months). Attenuation characteristics, safety margin, and congruency had no significant effect on the probability of local tumor progression. Coagulations whose margin was categorized as "discontinuous" were significantly more often associated with local recurrence ($p = 0.038$). No significant influence on local recurrence could be detected regarding coagulation shape, margin distinction, and configuration.
Conclusion: Computed tomography imaging immediately after RF ablation allows for morphological characterization of the coagulation and provides a valid baseline status for follow-up imaging. However, in CRM, morphological image criteria and attenuation characteristics have limited predictive value for immediate detection of persistent tumor.

Key words: Radiofrequency ablation—Computed-tomography—Liver—Colorectal cancer metastasis—Treatment control

Colorectal cancer (CRC) represents the fourth most common solid tumor worldwide [1]. Most CRC deaths result from metastasis and, in many patients, the liver is the first and the only site of metastatic spread [2]. However, only 10–20% of all patients meet the requirements for surgical treatment [3]. Radiofrequency (RF) ablation is accepted as an established local therapeutic modality in the treatment of malignant hepatic tumors that considerably improves the survival rates of patients with unresectable liver metastases [2, 4–7]. However, local recurrence—mostly situated along the peripheral margin of the RF-induced coagulation—remains a major challenge of RF ablation [8]. Inter- and intra-tissue variability due to the different thermal and electrical conductivity of the tissues combined with the risk of suboptimal placement of the RF applicator may lead to insufficient heating distribution and thus to persistence of viable tumor cells after therapy. Waiting until local tumor growth becomes manifest carries a high risk of further metastatic spread [9]. Thus, ablative treatment success is strongly dependent

Correspondence to: Christina Schraml; *email:* christina.schraml@med.uni-tuebingen.de

on ensuring complete tumor destruction and requires excellent monitoring [9, 10]. However, there is no clear consensus as to which imaging technique is most suitable for the evaluation of ablation results. To date, contrast-enhanced computed tomography (CT) has been the most widely used imaging modality in the evaluation of the therapeutic response after RF ablation [11]. Several studies have been performed to evaluate the diagnostic performance both for colorectal metastases (CRM) and hepatocellular carcinoma (HCC) [9, 10, 12–15]. However, these studies are mainly focusing on image findings that are present later in the follow-up controls. Furthermore, assessment of ablation completeness is probably more complicated in cases of CRM than in HCC, mainly due to their infiltrative growth and the lack of tumor capsule.

To our knowledge, no study has been performed dealing with the diagnostic performance of contrast-enhanced CT obtained immediately after RF treatment in cases of hepatic CRM. As contrast-enhanced CT scans are routinely obtained as a final control after each intervention in many institutions, it is important to investigate their diagnostic significance regarding immediate detection of persistent viable tumor.

Therefore, the goal of the present study was to assess the accuracy of CT in the evaluation of RF treatment efficacy immediately after RF ablation of CRM.

Methods

Patients

The study was conducted in accordance with the guidelines of the local institutional review board. Written informed consent was obtained from all subjects. Since 2000, 89 patients with CRC and liver metastasis received image-guided percutaneous hepatic RF ablation therapy in our institution. 26 of them (18 men, 8 women, mean age: 62.9 ± 8.8 years, age range: 39–82 years) were treated under CT-guidance for 38 hepatic metastases. In 21 patients one single lesion was treated, in 4 patients 2 lesions were treated, in one patient 4 lesions were treated, and in one patient 5 lesions either in one or in multiple sessions were treated. In accordance with current practice, results of follow-up imaging, histopathology, and clinical and laboratory parameters including tumor markers were used to verify the absence/presence of residual or recurrent viable tumor, so-called "local tumor progression" as defined in terminology and reporting criteria established by the international working group of image-guided tumor ablation [16]. The mean general observation period including all other available imaging modalities as well as clinical follow-up ranged between 63 and 1203 days (mean: 499 ± 393 days).

RF ablation procedure

All percutaneous RF ablations were performed by the same two experienced interventional radiologists using a RF generator with a maximum power of 200 W coupled to an internally cooled single ($n = 15$) or cluster ($n = 23$) RF applicator (Cool Tip, Valleylab, Burlington, CO). The cluster applicator consisted of three parallel internally cooled single electrodes spaced 0.5 cm apart and grouped equidistantly in a triangle. Length of the applicator was 15 cm with a non-isolated active tip of 2.5 cm (cluster) or 3 cm (single). For energy deposition, the standard protocol recommended by the manufacturer was implemented. Two (single applicator) or four grounding pads (cluster applicator) were applied to the patient's thighs and back. RF current was emitted with the generator set to deliver the maximum power in the impedance control mode. All 38 metastases were treated according to protocol. Single ($n = 18$) or overlapping ($n = 20$) percutaneous ablations were performed on the basis of CT image findings performed during the ablation course. The evaluation of technical success was based on the immediate postinterventional images. In all cases, applicator repositioning and additional ablations were performed until visible tumor was supposed to be covered completely. After each ablation, cauterization of the needle track was performed during repositioning and retraction of the applicator.

CT imaging

Computed tomography scans were performed on a Somatom Sensation 16 (Siemens, Medical Solutions, Erlangen, Germany) scanner before, during, and immediately after RF energy deposition. The protocol included non-enhanced as well as contrast-enhanced CT scans in the portal venous phase (after 60 s delay) after administration of 1.2 mL per kg body weight of an iodinated contrast agent (Ultravist 300®, 0.623 g iopromid mL, 300 mg iodine/mL, Schering, Germany) at a flow rate of 3 mL/s, resulting in a total dose of 2.4 mL per kg body weight for each patient (pre- and post-ablative scan). Applicator placement was performed on non-enhanced images. CT images of the liver were acquired in a supine position using a 16×0.75 mm collimation, 120 kV and 170 mAs. A slice thickness of 5 mm was chosen for visualization, image matrix was 512×512.

Image evaluation

Quantitative evaluation. Image evaluation of pre-contrast and portal phase CT scans was performed by a consensus of three radiologists experienced in liver imaging after RF ablation who were blinded to the follow-up results. In all cases, CT scans before and immediately after RF treatment were evaluated and compared. Tumor and coagulation size were assessed based on measurements of both short-axis and long-axis diameters.

To assess for completeness of the ablation, safety margin was assessed in four quadrants by comparing the
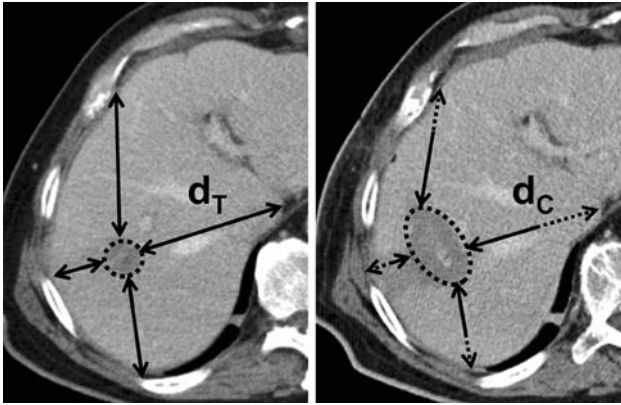
Fig. 1. Assessment of safety margin. To assess for completeness of the ablation, the safety margin was assessed in four quadrants by comparing the distance from the margin (*dashed circle*) of the tumor (d_T in the left scan obtained prior to RF ablation) and the coagulation zone (d_C in the right scan obtained after RF ablation) to placed basing points. Safety margin in each direction was then calculated as the difference d between the two distances: $d = d_T - d_C$.
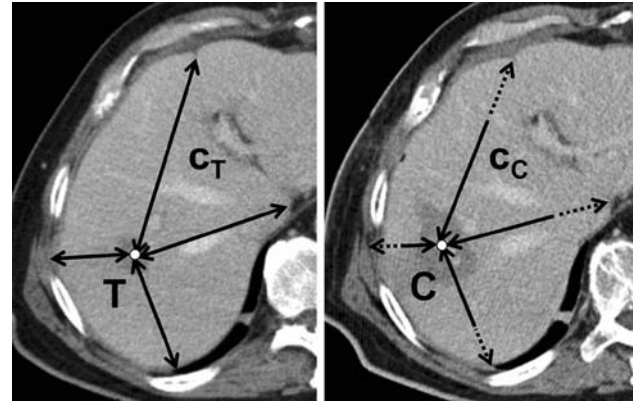

Fig. 2. Assessment of lesion congruency. To verify the congruency of tumor (T) and coagulation zone (C) the distance between the center point of tumor (c_T in the left scan obtained prior to RF ablation) and coagulation zone (c_C obtained after RF ablation) was assessed in four different directions. The center points were defined by the intersection point of long- and short-axis of the lesion. Deviation c of the two center points T and C in each direction was quantified by comparing the distances from the tumor's and coagulation's center point to placed basing points: $c = c_c - c_T$.

distance from the margin of the tumor (d_T) and the coagulation (d_C), respectively, to placed basing points, e.g., portal vessel bifurcation, liver capsule constriction, cysts, or other distinctive anatomical structures (Fig. 1). Safety margin was calculated as the difference d between the two distances: $d = d_T - d_C$. For statistical analysis, the smallest value of the distances assessed in four quadrants was taken into account.

To verify the congruency of tumor and ablation zone, the distance between the center point of tumor (T) and coagulation zone (C) to placed basing points (defined as c_T and c_C) was assessed in four different directions (Fig. 2). The center points were defined by the intersection point of long- and short-axis of the lesion. Deviation c of T and C in each direction was quantified by comparing the distances from the tumor's and coagulation's center points to placed basing points, respectively: $c = c_C - c_T$. For statistical analysis, the greatest distance between the two center points was taken into account.

Attenuation characteristics. Post-ablational so-called "pre-contrast" images were obtained prior to final contrast-enhanced control scan. In fact, those images were not completely "pre-contrast," because parenchyma partially stored reduced amounts of contrast agent that had been applied during targeting. For data analysis, this was considered by introducing ratios referring attenuation values of the lesions to surrounding liver parenchyma. Calculation of ratios was based on measurements of contrast enhancement (CE) by applying regions of interest (ROI) inside the tumor (r_T), respectively the coagulation zone (r_C) and an area of normal liver parenchyma. Ratios were determined as follows:

$$r_T = \frac{\text{CE of tumor}}{\text{CE of normal liver parenchyma}}$$

$$r_C = \frac{\text{CE of coagulation}}{\text{CE of normal liver parenchyma}}$$

The lesions' attenuation values (mean, minimum, and maximum values in the ROI) inserted in the equations are quantified in Hounsfield units. In order to balance tissue inhomogeneities, mean attenuation value gathered from four round-shaped different ROIs of 1 cm^2 was calculated. If the tumor was smaller than 1 cm^2, the ROI size was adapted accordingly, so that it covered the whole tumor. The ROIs were carefully placed inside the ablation zone avoiding the central carbonization zone. In order to particularly investigate changes in attenuation values due to tissue changes related to the ablation procedure, the difference between r_T and r_C was calculated and statistically analyzed.

Qualitative evaluation. In addition, qualitative analysis of the coagulation zone was performed on portal phase scans.

The morphology of the coagulation's marginal zone was classified by the following criteria:

Coagulation shape. The shape of the coagulation zone was classified in two groups. If the coagulation zone had a clearly round or oval, non-lobulated shape it was classified as "regular" (Fig. 3A) otherwise the zone was categorized as "irregular" (Fig. 3B–D).
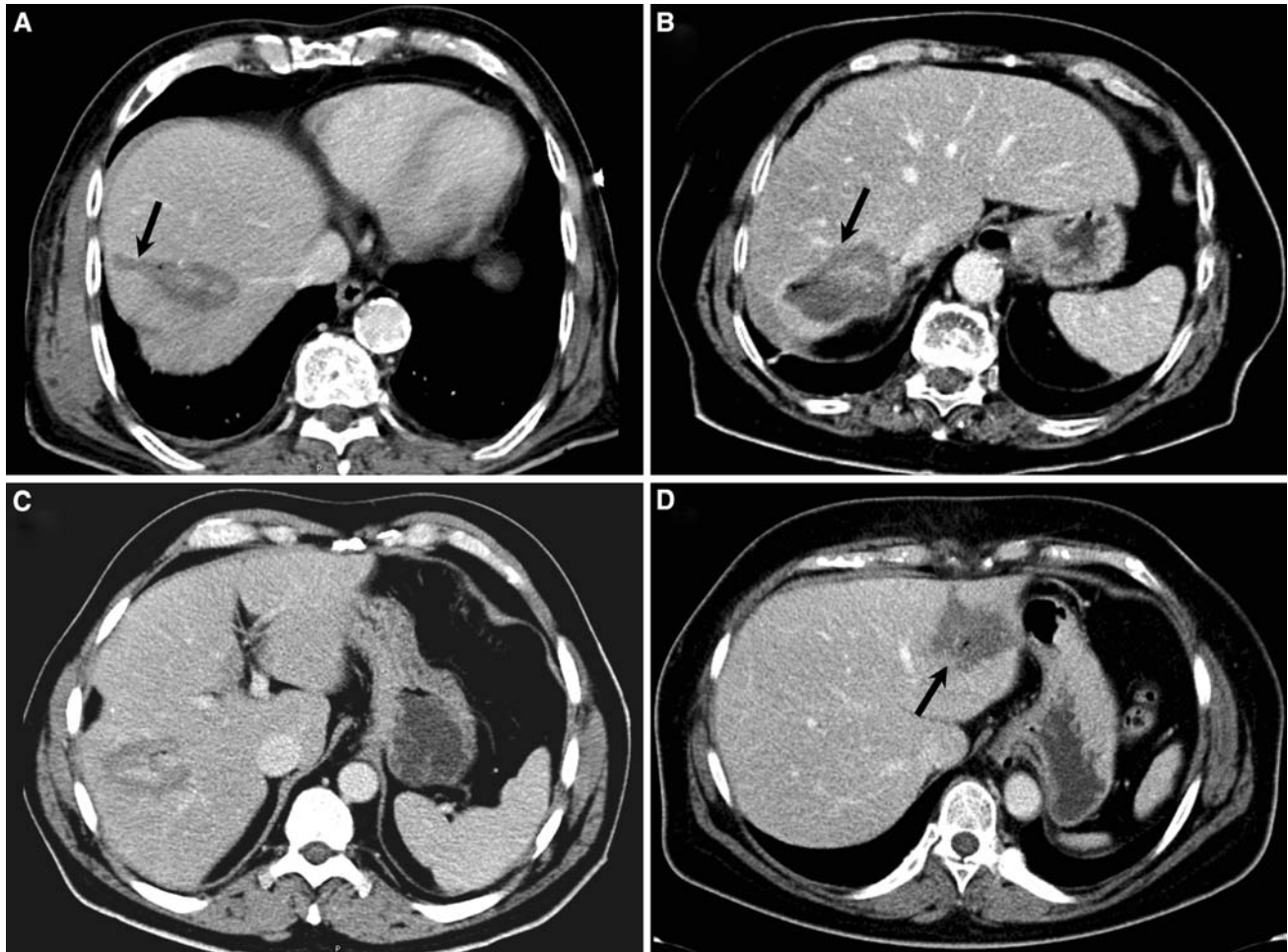
Fig. 3. Portal phase CT scans illustrating different features of coagulation zones. **A** Coagulation zone classified as regular, sharply distinguishable, and strictly circular. A continuous margin can be depicted around the circumference of the hypodense coagulation zone. The linear extension on the right border depicts the coagulated needle track (*arrow*). **B** Coagulation zone categorized as diffusely distinguishable and irregular shaped. The *black arrow* depicts the discontinuity of margin course. Reactive hyperemia can be observed in the adjacent liver parenchyma. **C** Diffusely distinguished, slightly irregular coagulation zone with central carbonization. **D** Irregular shaped, diffusely distinguished coagulation zone. The margin was exhibiting a nodule (*arrow*), accordingly margin was classified as discontinuous.

Margin distinction. A sharply distinguishable transition between coagulation zone and surrounding liver parenchyma was classified as "well-defined" (Fig. 3A and B), if the transition zone was broad and blurred, the margin aspect was classified as "diffuse" (Fig. 3C and D).

Margin configuration. The margin configuration was analyzed with regard to presence of nodules emerging out into the hypodense area of the coagulation zone. An example for a nodule is marked by the black arrow in Fig. 3D. If no nodules were observed, the margin configuration was categorized as "strictly circular."

Margin continuity. The peripheral transition zone surrounding the coagulation zone was assessed with regard to continuity. It was classified as "continuous" (Fig. 3A) if margin course was clearly traceable along the whole circumference of the coagulation area; if the margin course was interrupted it was classified as "discontinuous" (Fig. 3B–D). Accordingly, all coagulation zones exhibiting a peripheral nodule were classified as discontinuous.

Statistical analysis

The data were analyzed using the statistical software JMP IN 5.1 (SAS Institute Inc., Cary NC, USA). Differences of tumor and coagulation size between portal phase scans and pre-contrast scans were analyzed by means of paired t-tests.

Paired t-tests were also used to compare r_T with r_C in the pre-contrast and in the portal phase scans.

To examine the effect of $r_T - r_C$ and of the morphology of the coagulation margin on the probability of

local tumor regrowth, nominal logistic regressions were performed. Due to the rather small sample size, only one factor was used for each logistic regression, together with the logarithm of the follow-up time as covariate.

Results

All metastases except one were detectable on pre-contrast scans; on portal phase scans all metastases were measurable. Typical pre- and post-ablative CT scans are shown in Fig. 4. Regarding the pre-ablative imaging, in one case, no pre-contrast scans and in two cases no portal phase scans were available. As to the post-ablative imaging, in two cases, no pre-contrast scans were available.

Technical effectiveness (defined as no evidence of local tumor progression at follow-up imaging 4 months after treatment) was achieved for 26 of 38 treated metastases (68%). In 12 ablations (32 %) local tumor progression was observed within 4 months after one single treatment session. In 24 cases, local tumor progression was present during the entire clinical follow-up time.

Quantitative image analysis

Tumor and coagulation size. The median (min–max) size of CRM assessed in the portal phase scan was found to measure 2.1 cm (0.6–5.2 cm) in the long axis and 1.7 cm (0.6–2.9 cm) in the short-axis diameter. The median size assessed in the pre-contrast scans was 1.9 cm (0.4–4.4 cm) in the long axis and 1.6 cm (0.4–3.9 cm) in the short axis. The median (min–max) size of coagulation zone assessed in the portal phase scan was found to
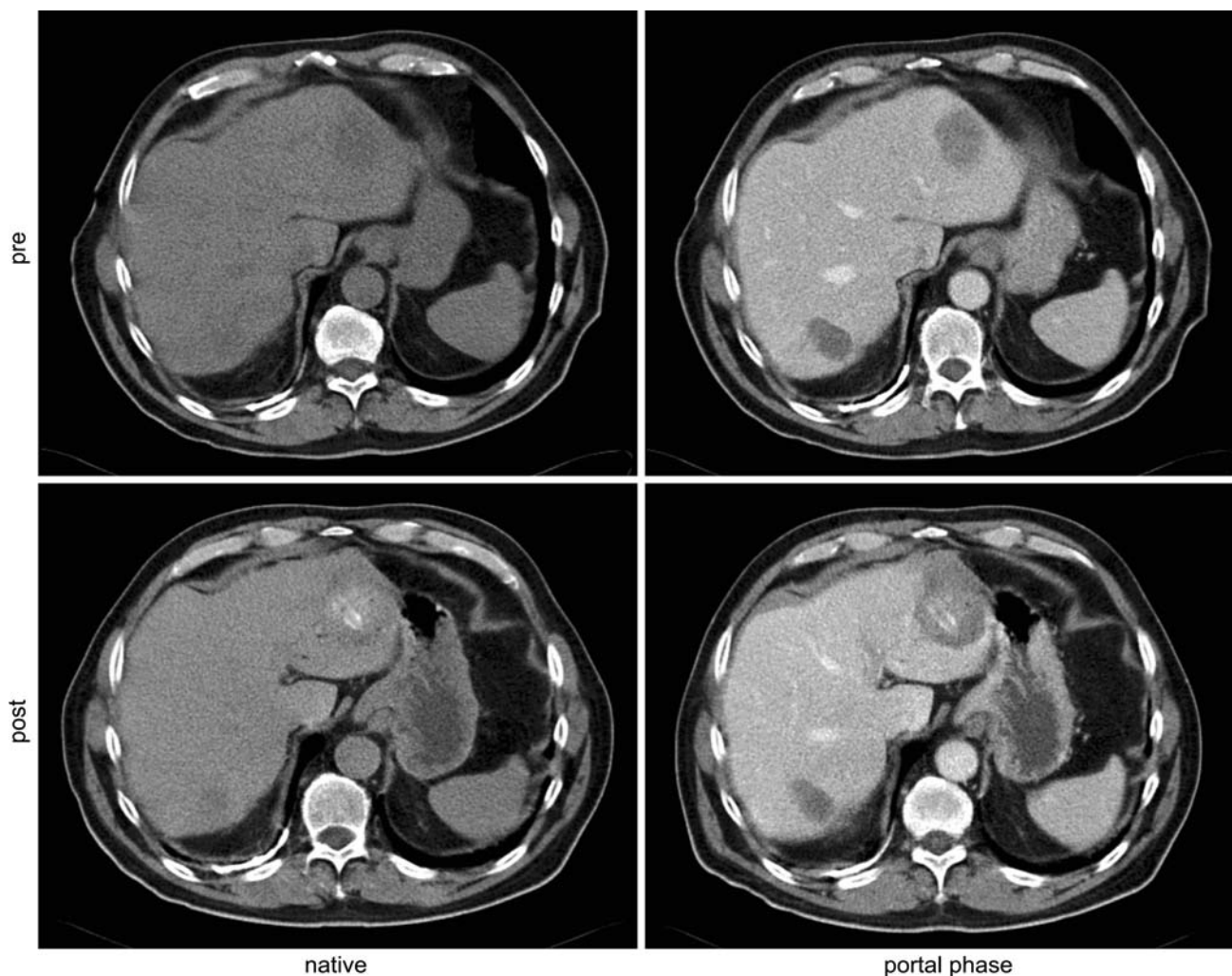

Fig. 4. 69-Year-old man with hepatic colon cancer metastasis in the left lobe. In the upper row, the pre-ablative pre-contrast (*left*) and portal phase scan (*right*) are shown. The corresponding post-ablative scans below depict an ill-defined, hypodense ablation area with central hyperdense carbonization zone. No prominent peripheral enhancement is noticed. No local tumor progression was observed in a follow-up period of 14 months. Note the zone of a previous successful ablation in the right lobe (segment VII).

measure 4.3 cm (1.6–7.5 cm) in the long axis and 2.9 cm (1.2–5.1 cm) in the short-axis diameter. The median size assessed in the pre-contrast scans was 3.5 cm (1.3–5.7 cm) in the long axis and 2.5 cm (1.1–4.4 cm) in the short axis.

Both tumor and coagulation extent measured in long and short axes were significantly larger in the portal phase scans than in the pre-contrast scans ($p < 0.05$ for both axes).

Attenuation characteristics. The calculated ratios for r_T and r_C in both the pre-contrast and the portal phase scan are summarized in Table 1. Both on pre-contrast and on portal phase scans, all lesions were hypodense compared with the surrounding liver parenchyma. On pre-contrast scans, coagulation zone appeared hypodense in 33 cases, hyperdense in two cases, and was isodense to the surrounding liver parenchyma in one case. On portal phase scans, coagulation zone was hypodense in 35 cases, hyperdense in two cases, and isodense in one case. No significant difference in attenuation changes (analyzed by calculating the difference: $r_T - r_C$) could be found between completely ablated lesions and the coagulation sites that presented local tumor progression.

Safety margin. Median (min–max) safety margins measured in four different quadrants were 0.5 (0–2.6), 0.5 (0–3.5), 0.6 (0–3.3), and 0.6 (0–3.5) cm which averages in a safety margin of 0.83 cm (range: 0–3.4 cm). The probability of local tumor progression was not affected by the safety margin. *p*-Values for the four quadrants were: 0.95, 0.57, 0.38, and 0.90. When analyzing the minimum safety values of all quadrants, no significant influence on local tumor progression could be detected ($p = 0.80$).

Congruency. Median (min–max) deviations between the center points of tumor and coagulation zone assessed in four directions were 0.4 (0–2.2), 0.4 (0–2.3), 0.4 (0–3.4),

and 0.2 (0–2.5) cm. The measured deviations had no significant effect on the probability of local tumor progression. *p*-Values for the four directions were: 0.40, 0.30, 0.10, and 0.30. When analyzing the maximum values of all directions, no significant influence on local tumor progression could be detected ($p = 0.19$).

Qualitative image analysis

Evaluation of the coagulation's morphology for all lesions together as well as divided into two groups (with and without local tumor progression) is summarized in Table 2. Coagulation zones whose peripheral margin was categorized as "discontinuous" were significantly more often associated with local tumor progression observed in the follow-up ($p = 0.038$). Coagulation zones classified as "irregular shaped" showed a tendency to higher relapse rates, even though no statistical significance was detected ($p = 0.06$). However, neither margin distinction ($p = 0.45$) nor margin configuration ($p = 0.70$) affected the probability of local tumor progression significantly.

Discussion

Radiofrequency ablation is the most widely used treatment option among minimally invasive techniques for limited metastatic disease in cases of unrespectable hepatic metastasis or relapse after surgical resection [16, 17]. Contrast-enhanced CT and magnetic resonance (MR) imaging are at present considered the most useful modalities for the assessment of treatment success at follow-up [11, 13]. Several studies have been performed dealing with the identification of local tumor progression after RF ablation in the follow-up imaging [8–10, 13, 15, 18, 19]. However, there are no established criteria for the evaluation of treatment success immediately after the intervention. Antoch et al. investigated the value of PET-CT in this aspect and conclude that information

Table 1. Attenuation characteristics

CT phase	r_T[a]	r_C[a]	$r_T - r_C$	Significant difference between r_T and r_C *p*-Value (paired *t*-test)	Probability of LTP *p*-Value (logistic regression)
Pre-contrast					
All	0.62 ± 0.17	0.76 ± 0.15	−0.11 ± 0.25		
LTP	0.63 ± 0.20	0.78 ± 0.16	−0.10 ± 0.28		
No LTP	0.60 ± 0.13	0.74 ± 0.16	−0.13 ± 0.20		
				0.0093[2]	0.7180[b]
Portal phase					
All	0.63 ± 0.17	0.68 ± 0.14	−0.08 ± 0.25		
LTP	0.62 ± 0.16	0.66 ± 0.13	−0.06 ± 0.25		
No LTP	0.65 ± 0.20	0.70 ± 0.17	−0.11 ± 0.26		
				0.0634	0.3197

LTP = local tumor progression
[a] For quantitative data analysis, ratios r_T and r_C were calculated for both scan phases by referring the attenuation values of tumor (T) and coagulation zone (C), respectively, to surrounding liver parenchyma
[b] Lesion #18 was excluded for calculation because the tumor was not detectable in the pre-contrast scans

Table 2. Morphological analysis of the coagulation zone

Evaluation of coagulation's morphology	All cases	Cases without LTP	Cases with local LTP	p-Value
Shape				0.06
Regular	15	8	7	
Irregular	23	6	17	
Margin distinction				0.45
Diffuse	13	6	7	
Well defined	24	8	16	
Not determinable	1	0	1	
Margin configuration				0.70
Strictly circular	28	11	17	
Presence of nodule	5	0	5	
Not determinable	5	3	2	
Margin continuity				0.038
Continuous	33	14	19	
Discontinuous	5	0	5	

LTP = local tumor progression
Summary of the morphological analysis of the coagulation zones
In the third and in the fourth column, a separate summary for the groups "no local tumor progression" and "local tumor progression" is given.
Statistical analysis (nominal logistic regression) was performed with regard to tumor regrowth; the corresponding p-values are given in the right column

regarding the tracer distribution around the area of necrosis might serve for immediate assessment of persistent tumor after RF treatment [9]. Dromain et al. reported a higher sensitivity in early detection of local tumor progression on MR imaging than on CT but without significant difference ($p = 0.12$) [13]. In clinical routine, however, it is not easily practicable to perform MR or PET-CT scans immediately after the CT-guided RF intervention, especially as the control should be performed with the patient still prepared so that retreatment can be performed instantly when persistence of viable tumor is suspected. Previous publications have indicated that contrast-enhanced ultrasound might be promising in the evaluation of treatment success [20]. However, this imaging modality is strongly operator dependent and it is much more difficult to perform a three-dimensional assessment from a transient ultrasound study than from multiplanar reformatting of a three-dimensional CT dataset [21].

Hepatic tumors show different CT enhancement patterns. HCC as well as metastases from neuroendocrine tumors typically present as lesions with early arterial contrast enhancement with a peripheral capsule [22]. In contrast, hepatic metastases from CRC are mostly imaged as hypoattenuating lesions, which are best visualized during the portal venous phase of liver enhancement [9, 23]. Therefore, in this study which focuses solely on CRM, portal phase scans were chosen for image evaluation.

Immediately after the intervention, transient hyperemia caused by outflow obstruction leads to increased contrast enhancement at the periphery of the coagulation zone, impairing detection of residual tumor if the tumor presents furthermore as hyperattenuating [14, 24]. When assessing patients with liver metastasis from tumors of the gastrointestinal tract, the typical rim enhancement is not expected to cause interpretative problems. A rim-like contrast enhancement that is not present on the pre-ablative image and is firstly observed after treatment can be attributed to reactive transient hyperemia and will not be mistaken for residual tumor. In our study, the typical post-ablative rim enhancement already described in other studies [14] was not very prominent. A possible explanation for this finding might be that the transient hyperemia that is surrounding the RF ablation zone may be more distinct in the arterial phase. Besides, one has to keep in mind, that the evaluated CT scans were obtained immediately after ablation before visible inflammatory response-related tissue changes are present. In addition, it has to be considered that, during one RF ablation session, contrast media is administered several times, so that not always the ideal amount of contrast media is injected for each scan in order to reduce possible advent effects especially renal toxicity.

Different morphologic criteria considering characterization of the coagulation's margin, margin morphology, and margin continuity, were defined. We could demonstrate that coagulation zones whose margins were categorized as "discontinuous" were significantly more often associated with local tumor progression than when classified as "continuous." However, no significant effect of coagulation shape, margin distinction, and margin configuration on local tumor progression could be detected. The discrepancy to reported studies confirming the diagnostic performance of CT in the assessment of RF treatment may be explained by the fact that those studies are based on images obtained at later follow-up intervals [10, 11, 25]. However, results of the present study suggest that evaluation of the coagulation's morphology immediately after ablation procedure has only limited predictive value in the assessment of ablation completeness with the exception of the criteria "discontinuity of margin."

In addition to qualitative analysis, we investigated RF-treatment-induced changes in the relative attenua-

tion values obtained in ROIs within the coagulation zone. Apart from the central hyperdense carbonization zone near the applicator shaft, both colorectal metastasis and coagulation zone do present as hypoattenuating lesions without inner contrast enhancement. To our knowledge, it has not been previously investigated as to whether there is a significant difference between density values of metastasis and coagulative tissue necrosis that might serve as a parameter for assessment of ablation completeness. We detected a slight but not significant increase in post-ablative attenuation values in all cases. This might be due to higher density values of coagulated blood that is present inside the coagulation zone. However, no significant difference in attenuation changes could be found between completely coagulated lesions and the coagulation sites that presented local tumor progression.

In 12 of 38 ablation zones (32%), residual tumor was detected after the first RF ablation session within four months after ablation (first patency). The reported local failure rates after RF ablation in the literature range from 2.3% to 40% [26–29]. A possible explanation for this variation may be the heterogeneity in the definition of endpoints and assessment of treatment effectiveness. Explicitly, in the present study, RF ablation was judged technically effective—as proposed by the International Working Group on Radiofrequency Ablation [16]—when no local tumor progression was detected in the first two imaging control examinations following the intervention (e.g., 4 months after ablation procedure). This rate of 32% may seem relatively high in comparison to other studies [2]. In addition, one has to consider that the calculated percentage of 32% does not reflect the final outcome of our patients, because several patients with detection of local tumor progression in the first imaging controls were retreated in further ablation sessions and complete tumor destruction could be achieved.

In current clinical practice, adequate ablation result is based on comparison between the size of the distinct hypovascular ablation zone on the immediate post-ablation CT and the size of the lesion on the pre-ablational CT [7]. However, presence and extent of a safety margin is difficult to estimate. The width of the ablative safety margin has been a permanent point of discussion not only in RF ablation, but also in liver surgery. Up to now, a safety margin of 5–10 mm in all directions around the tumor is generally accepted by most surgeons and pathologists [30]. On the other hand, some studies conclude that the width of the resection margin does not influence the post-operative recurrence rate or pattern of recurrence [31]. In the present study, the probability of local progression was not affected by the assessed safety margin. Probably the tumor biology itself plays an important role regarding local tumor progression rate.

In addition to comparison between tumor and coagulation dimensions, it is further essential to confirm a certain congruency of tumor site and localization of the coagulation zone. Hence, we additionally investigated the distances between the center points of the tumor and the coagulation zone. However, findings of the present study suggest, that neither assessment of safety margin nor evaluation of congruency immediately after the RF-procedure improved diagnostic performance with regard to local tumor progression. These results should not be misinterpreted. It is obvious, that assuring a certain safety margin and congruency of lesion and coagulation zone may influence treatment efficacy. The missing statistical significance with regard to predicting tumor progression demonstrates rather that evaluation of image information obtained immediately after RF ablation has limitations. Furthermore, precise section-by-section comparison is difficult if section positions and orientations do not match exactly between pre- and post-ablational CT examinations. The use of multiplanar reformations may help, but analyzing many images of different slices can be very time-consuming, and is therefore not feasible in clinical routine. However, the aim of this study was to analyze the predictive value of evaluation methods that are easy to apply in clinical routine. The application of software-based evaluation tools that allow for fast automatical lesion segmentation and fusion of pre- and post-ablational images could markedly improve evaluation of RF ablation therapy [32].

Limitations of our study include the relatively small number of patients and lesions. But as we focused on one tumor entity that shows homogeneous appearance in CT imaging reliable statistical analysis is warranted. In this study, we focused on CRM because it is the most frequent secondary liver malignancy and is likely to be one of the most difficult tumor types to be evaluated at CT after RF ablation because of their hypodense character.

As the following study is based on the evaluation of axial images, possible influence of partial volume effects on distinctiveness of margin could not be completely excluded. Besides, a defined observation period was not realizable due to individual course of disease and retreatment in each patient. Differences in the follow-up times were therefore considered in the statistical analysis. As histological proof or exclusion of tumor recurrence was not available in all patients, results of follow-up imaging and clinical features including laboratory parameters were used to determine whether an ablation was complete or incomplete. This was done in line with current practice [5, 33].

Conclusion

Computed tomography imaging performed immediately after RF ablation allows for morphological characterization of the coagulation zone as well as assessment of the coagulation extent and provides a valid baseline status for further follow-up imaging. However, in CRM,

analysis of quantitative CT criterion like safety margin, congruency between lesion and coagulation zone, and attenuation characteristics has limited significance regarding immediate detection of persistent viable tumor. Only the criteria "discontinuity of margin" seems to be a valid tool for reliable assessment of the marginal area at risk of tumor residual.

References

1. Jemal A, Siegel R, Ward E, et al. (2006) Cancer statistics, 2006. CA Cancer J Clin 56(2):106–130
2. Livraghi T, Solbiati L (2001) [Percutaneous treatment: radiofrequency ablation of hepatic metastases in colorectal cancer]. Tumori 87(1 Suppl 1):S69
3. Manfredi S, Lepage C, Hatem C, et al. (2006) Epidemiology and management of liver metastases from colorectal cancer. Ann Surg 244(2):254–259
4. Pereira PL (2007) Actual role of radiofrequency ablation of liver metastases. Eur Radiol 17(8):2062–2070
5. Solbiati L, Livraghi T, Goldberg SN, et al. (2001) Percutaneous radio-frequency ablation of hepatic metastases from colorectal cancer: long-term results in 117 patients. Radiology 221(1):159–166
6. Rhim H, Goldberg SN, Dodd GD 3rd, et al. (2001) Essential techniques for successful radio-frequency thermal ablation of malignant hepatic tumors. Radiographics 21 Spec No:S17–S35; discussion S36–S19
7. Barker DW, Zagoria RJ, Morton KA, et al. (2005) Evaluation of liver metastases after radiofrequency ablation: utility of 18F-FDG PET and PET/CT. AJR Am J Roentgenol 184(4):1096–1102
8. Kim YS, Rhim H, Cho OK, et al. (2006) Intrahepatic recurrence after percutaneous radiofrequency ablation of hepatocellular carcinoma: analysis of the pattern and risk factors. Eur J Radiol 59(3):432–441
9. Antoch G, Vogt FM, Veit P, et al. (2005) Assessment of liver tissue after radiofrequency ablation: findings with different imaging procedures. J Nucl Med 46(3):520–525
10. Kim SK, Lim HK, Kim YH, et al. (2003) Hepatocellular carcinoma treated with radio-frequency ablation: spectrum of imaging findings. Radiographics 23(1):107–121
11. Chopra S, Dodd GD 3rd, Chintapalli KN, et al. (2001) Tumor recurrence after radiofrequency thermal ablation of hepatic tumors: spectrum of findings on dual-phase contrast-enhanced CT. AJR Am J Roentgenol 177(2):381–387
12. Ninomiya T, Seo Y, Yano Y, et al. (2006) Evaluation of the therapeutic effect using MD-CT immediately after RFA for HCC. Hepatogastroenterology 53(70):558–560
13. Dromain C, de Baere T, Elias D, et al. (2002) Hepatic tumors treated with percutaneous radio-frequency ablation: CT and MR imaging follow-up. Radiology 223(1):255–262
14. Limanond P, Zimmerman P, Raman SS, et al. (2003) Interpretation of CT and MRI after radiofrequency ablation of hepatic malignancies. AJR Am J Roentgenol 181(6):1635–1640
15. Tsuda M, Rikimaru H, Majima K, et al. (2003) Time-related changes of radiofrequency ablation lesion in the normal rabbit liver: findings of magnetic resonance imaging and histopathology. Invest Radiol 38(8):525–531
16. Goldberg SN, Grassi CJ, Cardella JF, et al. (2005) Image-guided tumor ablation: standardization of terminology and reporting criteria. Radiology 235(3):728–739
17. Gillams AR, Lees WR (2004) Radio-frequency ablation of colorectal liver metastases in 167 patients. Eur Radiol 14(12):2261–2267
18. Aliberti C, Soriani M, Tilli M, et al. (2004) Radiofrequency ablation of liver malignancies: MRI for evaluation of response. J Chemother 16(Suppl 5):79–81
19. Veit P, Antoch G, Stergar H, et al. (2006) Detection of residual tumor after radiofrequency ablation of liver metastasis with dual-modality PET/CT: initial results. Eur Radiol 16(1):80–87
20. Meloni MF, Livraghi T, Filice C, et al. (2006) Radiofrequency ablation of liver tumors: the role of microbubble ultrasound contrast agents. Ultrasound Q 22(1):41–47
21. Gillams AR, Lees WR (2005) Radiofrequency ablation of colorectal liver metastases. Abdom Imaging 30(4):419–426
22. Paul SB, Gulati MS (2002) Spectrum of hepatocellular carcinoma on triple phase helical CT: a pictorial essay. Clin Imaging 26(4):270–279
23. Chiang SH, Thng CH, Teh CS, et al. (2003) Computed tomographic appearance of colorectal hepatic metastases. Ann Acad Med Singapore 32(2):191–195
24. Goldberg SN, Gazelle GS, Mueller PR (2000) Thermal ablation therapy for focal malignancy: a unified approach to underlying principles, techniques, and diagnostic imaging guidance. AJR Am J Roentgenol 174(2):323–331
25. Anderson GS, Brinkmann F, Soulen MC, et al. (2003) FDG positron emission tomography in the surveillance of hepatic tumors treated with radiofrequency ablation. Clin Nucl Med 28(3):192–197
26. van Duijnhoven FH, Jansen MC, Junggeburt JM, et al. (2006) Factors influencing the local failure rate of radiofrequency ablation of colorectal liver metastases. Ann Surg Oncol 13(5):651–658
27. Ng KK, Poon RT (2005) Radiofrequency ablation for malignant liver tumor. Surg Oncol 14(1):41–52
28. Sutherland LM, Williams JA, Padbury RT, et al. (2006) Radiofrequency ablation of liver tumors: a systematic review. Arch Surg 141(2):181–190
29. Jiao LR, Hansen PD, Havlik R, et al. (1999) Clinical short-term results of radiofrequency ablation in primary and secondary liver tumors. Am J Surg 177(4):303–306
30. Cady B, Jenkins RL, Steele GD Jr., et al. (1998) Surgical margin in hepatic resection for colorectal metastasis: a critical and improvable determinant of outcome. Ann Surg 227(4):566–571
31. Hamady ZZ, Cameron IC, Wyatt J, et al. (2006) Resection margin in patients undergoing hepatectomy for colorectal liver metastasis: a critical appraisal of the 1 cm rule. Eur J Surg Oncol 32(5):557–563
32. Bricault I, Kikinis R, Morrison PR, et al. (2006) Liver metastases: 3D shape-based analysis of CT scans for detection of local recurrence after radiofrequency ablation. Radiology 241(1):243–250
33. Choi H, Loyer EM, DuBrow RA, et al. (2001) Radio-frequency ablation of liver tumors: assessment of therapeutic response and complications. Radiographics 21 Spec No:S41–S54